NUCL SCI TECH (2017) 28:24
DOI 10.1007/s41365-016-0169-4

Non-destructive study of fruits using grating-based X-ray imaging

Sheng-Xiang Wang[1] · Ren-Fang Hu[1] · Kun Gao[1] · Faiz Wali[1] · Gui-Bin Zan[1] · Da-Jiang Wang[1] · Zhi-Yun Pan[1] · Shi-Qiang Wei[1]

Received: 14 June 2016 / Revised: 19 September 2016 / Accepted: 9 October 2016 / Published online: 28 December 2016

Abstract Grating-based X-ray imaging can make use of conventional tube sources to provide absorption, refraction and scattering contrast images from a single set of projection images efficiently. In this paper, a fresh cherry tomato and a dried umeboshi are imaged by using X-ray Talbot–Lau interferometer. The seed distribution in the scattering image of the cherry tomato, and the wrinkles of epicarp in the refraction image of the umeboshi, are shown distinctly. The refraction and scattering images provide more information on subtle features than the absorption image. Also, the contrast-to-noise ratio values show distinguishing capacity of the three kinds of imaging techniques. The results confirm that grating-based X-ray imaging is of great potential in non-destructive fruit testing.

Keywords Non-destructive testing · X-ray imaging · Talbot–Lau interferometer · Fruit testing

This work was supported by Japan-Asia Youth Exchange program in Science administered by the Japan Science and Technology Agency, the National Basic Research Program of China (No. 2012CB825801), and the National Natural Science Foundation of China (Nos. 11505188 and 11179004).

✉ Da-Jiang Wang
wdj@ustc.edu.cn

✉ Zhi-Yun Pan
zhypan@ustc.edu.cn

[1] National Synchrotron Radiation Laboratory, University of Science and Technology of China, Hefei 230029, China

1 Introduction

Non-destructive food testing plays an important role in food sieving and to guarantee high quality of food production. Most of the existing X-ray sieving machines [1] for vegetables and fruits use high X-ray absorption contrast to distinguish the foods and foreign matters, like stones and metals. However, X-ray sieving machines cannot function if foreign matters and foods have similar X-ray attenuation [2]. Owing to high evolution in X-ray imaging techniques during the past decade, as an X-ray grating-based imaging technique [3–8], Talbot interferometry and Talbot–Lau interferometry offer refraction and scattering signals to provide useful information on internal structures for understanding characteristics of the samples, becoming an important technique for food science [9]. Furthermore, with the use of source grating, this method can be operated with conventional X-ray source, instead of relying on brilliant synchrotron X-ray source. Thus, it is quite suitable for medical imaging and industrial non-destructive testing [10–15].

In this paper, we use a Talbot–Lau interferometer to obtain absorption, refraction and scattering contrast images of a fresh cherry tomato and a dry umeboshi. As for some other non-destructive methods, like VIS/NIR spectroscopy [16] and hyperspectral imaging [17], they mainly focused on fruit quality assessment using surface layer information but internal structure information of the fruits. Using penetration power of X-rays, the three complementary images provide internal structures information of the samples, hence the capability of this method for non-destructive fruit testing.

2 Experiment and methods

Experiments were carried out at the Institute of Multidisciplinary Research for Advanced Materials, Tohoku University, Japan, using a rotating anode X-ray tube in Talbot–Lau interferometer configuration, which is shown schematically in Fig. 1 [18]. A micro-focus X-ray generator with source grating (G0) is used for partially coherent illumination, in its acceleration voltage of 40 kV, the filament current of 45 mA and the X-ray spot size of 0.3 mm × 0.3 mm. The G0 grating was in 22.7-μm periods, the $\pi/2$ phase shift grating (G1) was in 4.36-μm periods and analyzer grating (G2) was in 5.4-μm periods. For the Talbot interferometer [19], the G0–G1 and G1–G2 distances were 106.9 and 25.6 cm, respectively. The gratings were optimized at the design photon energy of 27 keV. The projection images were recorded by a CCD detector (Special Instrument Inc.) with an effective receiving area of 68.4 mm × 68.4 mm in pixel size of 18 μm × 18 μm.

A fresh cherry tomato and a dried umeboshi were placed in a sample stage at upstream side of the phase grating G1. The measurements were carried out with air as a reference. Phase stepping [4] was used in this setup. The absorption grating G2 was scanned along the transverse direction X (Fig. 1) over one period of the grating. Five phase steps were used in both sample and reference measurements. At each phase step, an image was taken with an exposure time of 10 s. For the two samples, the experimental parameters were the same, at similar temperature and air humidity.

The shifting curve visibility of $V = 29.9\%$ was calculated using the mean intensity in the five steps in Fig. 2a. A Moire fringe always formed as two reasons, one is the superposition between the self-image of G1 and G2 pattern in the plane of the X-ray detector, and another is the mechanical errors of the gratings. The Moire fringe in Fig. 2b tends to be caused by mechanical errors of the gratings, and this problem can be solved through background subtraction in the data post-processing. The absorption $A(x, y)$, refraction $\theta(x, y)$ and scattering $V(x, y)$ signals of the sample were retrieved by Eqs. (1)–(3) [20]:

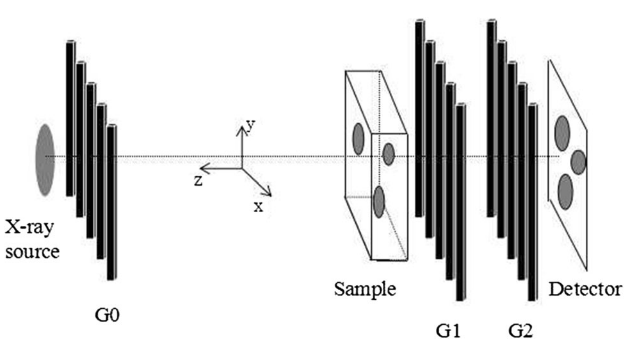

Fig. 1 Schematics of the X-ray grating interferometer (Talbot–Lau interferometer). A micro-focus X-ray generator is used with source grating (G0). G1 is for phase grating and G2 is for amplitude grating

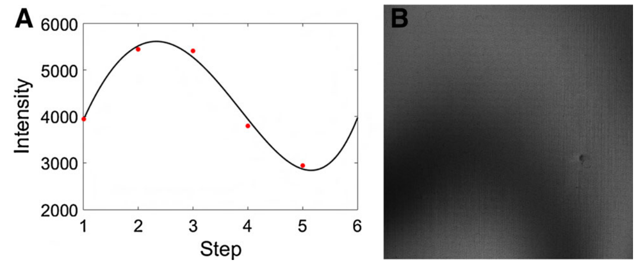

Fig. 2 Matched phase-step curve (**a**) with mean intensity value (the *red dots*) in five steps, and intensity image of Step 1 (**b**). (Color figure online)

$$A(x,y) = -\ln\left[\sum I_k^s(x,y)/\sum I_k^b(x,y)\right] \quad (k = 1,2,3,4,5), \tag{1}$$

$$\theta(x,y) = (d_2/2\pi Z)\arg\left[\sum I_k^s(x,y)e^{2\pi k/5}/\sum I_k^b(x,y)e^{2\pi k/5}\right] \quad (k = 1,2,3,4,5), \tag{2}$$

$$V(x,y) = \left[\sum I_k^b(x,y)/\sum I_k^s(x,y)\right]\mathrm{rem}\left[\sum I_k^s(x,y)e^{2\pi k/5}\right] /\mathrm{rem}\left[\sum I_k^b(x,y)e^{2\pi k/5}\right] \quad (k = 1,2,3,4,5), \tag{3}$$

where k is the number of steps during the phase stepping scan in one period of G2; $I_k^s(x,y)$ and $I_k^b(x,y)$ are the gray value of pixels at each step of the scan with and without the specimen, respectively; d_2 is the period of grating G2; and Z is the distance between grating G1 and G2.

3 Results and discussion

Figure 3 shows the photograph and grating-based X-ray images of the fresh cherry tomato. Structures of the cherry tomato, from the outer to the inner, are epicarp, mesocarp, endocarp and seeds. Epicarp is a botanical term for the outermost layer of the fruit, endocarp is an interior layer which directly surrounds the seeds and mesocarp is the fleshy middle layer between epicarp and endocarp. In the absorption image (Fig. 3b), along with the indistinct pedicel, the steady thickness increase from epicarp to the sample inner replies to the increase in X-ray absorption, with the gray values taking on degressive tendency. In the refraction image (Fig. 3c), the outer part of fruit stem, epicarp and some of the inner seeds can be distinguished, although the shape and the distribution of the seeds are not clear. Remarkably, not only the outer part of fruit stem but also inner part of stem can be observed clearly. Thanks to

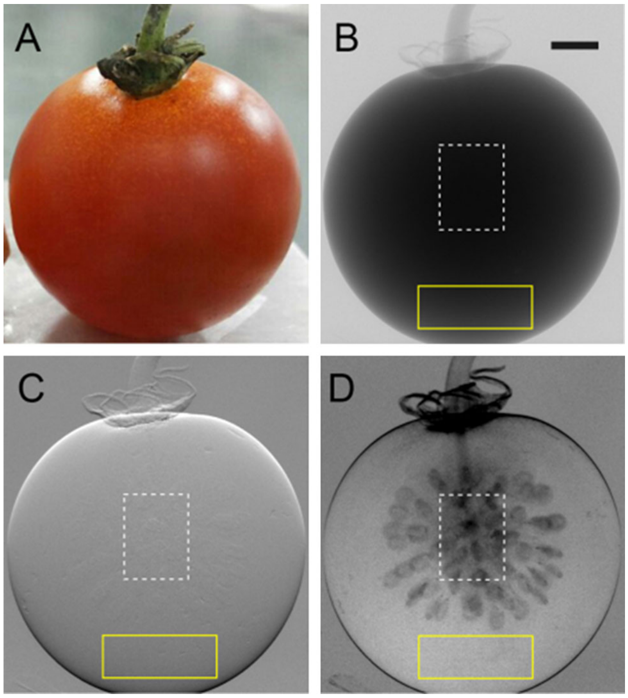

Fig. 3 A fresh cherry to (**a**) and its X-ray images of absorption (**b**), refraction (**c**), and scattering (**d**). *Scale bar* 3 mm

the large difference of gray value between mesocarp/endocarp and seeds, the size, position and direction of each seed can be distinguished, and the overlap place among seeds helps to understand stratification distribution of seeds in the scattering image (Fig. 3d).

Figure 4 provides the photograph and grating-based X-ray images of the umeboshi, one kind of dried fruit. Structures of umeboshi, from the outer to the inner, are epicarp, mesocarp, endocarp and seed. The boundary of endocarp and seed can be distinguished from the sample in absorption image (Fig. 4b), because the lignified endocarp is of lower density than mesocarp and the endocarp-seed

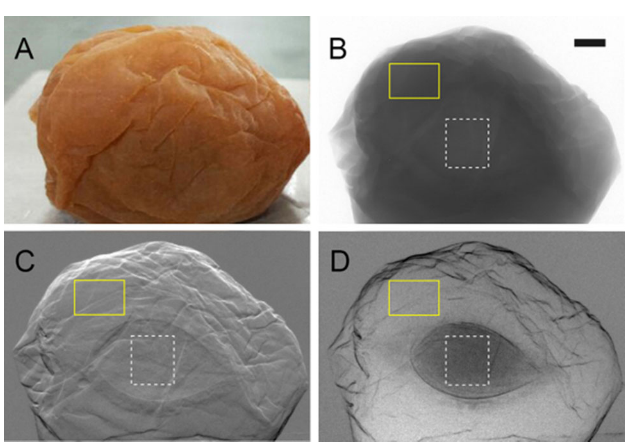

Fig. 4 A dried umeboshi (**a**) and its X-ray images of absorption (**b**), refraction (**c**), and scattering (**d**). *Scale bar* 2 mm

interspace produces a low gray value. By contrast, wrinkles on epicarp and section thickness of endocarp can be observed clearly in Fig. 4c for the refraction contrast. It is worth noting that in the scattering image (Fig. 4d), the hard lignified endocarp becomes fuzzy as low scattering signals, which exaggerate the seed obviously. Also, scattering signals from the endocarp are a little higher than those from the mesocarp, and this helps to find its position. It is exciting to find that the refraction image reveals details of the lignified endocarp, while the scattering image highlights characteristics of the seed, including the shape, size, and some other details. Therefore, the three X-ray images of different contrast provide complementary structure information of the dried umeboshi.

The traditional X-ray non-destructive imaging can only obtain the absorption information, which is strongly related to the sample thickness and density. The absorption value is larger with a thicker sample, and the inner signal is drawn in the whole signal group if the internal structures are of similar density. That is why seed structures of the cherry tomato are not shown in Fig. 3b, but the umeboshi endocarp and seed with density difference are observed in Fig. 4b.

Using the grating-based X-ray imaging, refraction and scattering images can be retrieved from the same set of projection data. They reproduce abundant information of surface and internal structures (Figs. 3c, d, 4c, d). The refraction image is sensitive to the density and refraction angles. This helps to reveal the seeds in the fresh cherry tomato and wrinkles on epicarp and the details of lignified endocarp in the dried umeboshi. The scattering signal is sensitive to the density and the reflection at the internal or external interfaces [21], which shows the seeds clearly in both fresh and dried fruits. Thus, all the internal structures that reflect the quality of fruits (fresh or dry) can be retrieved distinctly. It demonstrates that the grating-based X-ray imaging has high potential for non-destructive food testing.

Furthermore, the contrast-to-noise ratio (CNR) [22] can quantify the contrast of the three kinds of images as follows:

$$\mathrm{CNR} = \frac{|\mu_1 - \mu_2|}{\sqrt{\omega_1 \sigma_1^2 + \omega_2 \sigma_2^2}}, \tag{4}$$

where μ is the mean value and σ^2 is the variance of selected region of interest (ROI) in the absorption, refraction, and scattering images. The variances are weighted with the factor ω which is given by the ratio of the number of pixels in the matrix. The subscripts 1 and 2 mean the area of boxes by the white dotted lines and the yellow lines, respectively, as given in Figs. 3 and 4. A high CNR value means a high contrast to noise, whereas a low value represents a low contrast. As shown in Table 1, the scattering images of the fresh cherry tomato and dried umeboshi have

Table 1 Contrast-to-noise ratios of ROI in Figs. 3 and 4

Materials	Absorption	Refraction	Scattering
Cherry tomato	2.72	3.84	5.03
Umeboshi	1.22	1.79	6.09

the largest CNR value, hence the highest contrast of the three kinds of images. Therefore, scattering imaging helps to distinguish different structures and materials more clearly than absorption and refraction imaging.

4 Conclusion

In this work, the grating-based X-ray imaging by Talbot–Lau interferometer was used to investigate the internal structures of fresh and dried fruits non-destructively. Together with the traditional absorption image, the refraction and scattering images reproduce abundant information of the surface and interface. The refraction information is always clear at the boundary of different structures as the existence of refraction angle. The scattering signals are clearly sensitive to status of a fruit, with the highest contrast-to-noise ratio of the three kinds of images. The information in scattering images reflects the quality of fruits on the morphology, indicating the high potential of this imaging technique to conduct non-destructive testing on fruits. Moreover, the 3D tomography of fruit research can be operated when scattering images in a series of different angles are taken. However, grating-based X-ray imaging is time-consuming now. Further work on grating interferometry scanning system with a number of line detectors, and sample-maneuvering mechanism, will make this non-destructive technique to be a practical implementation in the near future.

Acknowledgements The authors would like to greatly appreciate Prof. Atsushi Momose and Dr. Margie P. Olbinado (Institute of Multidisciplinary Research for Advanced Materials, Tohoku University, Japan) for their kind help in conducting the experiments.

References

1. M. Graves, A. Smith, B. Batchelor, Approaches to foreign body detection in foods. Trends Food Sci. Technol. **9**, 21 (1988). doi:10.1016/S0924-2244(97)00003-4
2. Q. Chen, C. Zhang, J. Zhao et al., Recent advances in emerging imaging techniques for non-destructive detection of food quality and safety. Trac-Trend Anal. Chem. **52**, 261 (2013). doi:10.1016/j.trac.2013.09.007
3. A. Momose, Phase-sensitive imaging and phase tomography using X-ray interferometers. Opt. Express **11**, 2303 (2003). doi:10.1364/OE.11.002303
4. T. Weitkamp, A. Diaz, C. David et al., X-ray phase imaging with a grating interferometer. Opt. Express **13**, 6296 (2005). doi:10.1364/OPEX.13.006296
5. A. Olivo, R. Speller, A coded-aperture technique allowing X-ray phase contrast imaging with conventional sources. Appl. Phys. Lett. **91**, 074106 (2007). doi:10.1063/1.2772193
6. Y.I. Nesterets, S.W. Wilkins, Phase-contrast imaging using a scanning-doublegrating configuration. Opt. Express **16**, 5849 (2008). doi:10.1364/OE.16.005849
7. F. Pfeiffer, M. Bech, O. Bunk et al., Hard X-ray dark-field imaging using a grating interferometer. Nat. Mater. **7**, 134 (2008). doi:10.1038/nmat2096
8. B. Yuan, W. Yan, G. Kun et al., Investigation of noise properties in grating-based X-ray phase tomography with reverse projection method. Chin. Phys. B **24**, 108702 (2015). doi:10.1088/1674-1056/24/10/108702
9. F. Mendoza, P. Verboven, H.K. Mebatsion et al., Three-dimensional pore space quantification of appletissueusing X-ray computed microtomography. Planta **226**, 559 (2007). doi:10.1007/s13197-011-0485-y
10. M. Stampanoni, Z. Wang, T. Thüring et al., The first analysis and clinical evaluation of native breast tissue using differential phase-contrast mammography. Investig. Radiol. **46**, 801 (2011). doi:10.1097/RLI.0b013e31822a585f
11. F. Pfeiffer, J. Herzen, M. Willner et al., Grating-based X-ray phase contrast for biomedical imaging applications. Z. Med. Phys. **23**, 176 (2013). doi:10.1016/j.zemedi.2013.02.002
12. A. Momose, W. Yashiro, K. Kido et al., X-ray phase imaging: from synchrotron to hospital. Philos. Trans. R. Soc. A **372**, 20130023 (2014). doi:10.1098/rsta.2013.0023
13. C. Kottler, F. Pfeiffer, O. Bunk et al., Grating interferometer based scanning setup for hard X-ray phase contrast imaging. Rev. Sci. Inst. **78**, 043710 (2007). doi:10.1063/1.2723064
14. M.S. Nielsen, T. Lauridsen, L.B. Christensen et al., X-ray dark-field imaging for detection of foreign bodies in food. Food Control **30**, 531 (2013). doi:10.1016/j.foodcont.2012.08.007
15. M. Ruiz-Yaniz, F. Koch, I. Zanette et al., X-ray grating interferometry at photon energies over 180 keV. Appl. Phys. Lett. **106**, 151105 (2015). doi:10.1063/1.4917293
16. B.M. Nicolai, K. Beullens, F. Bobelyn et al., Nondestructive measurement of fruit and vegetable quality by means of NIR spectroscopy: a review. Postharvest Biol. Technol. **46**, 99 (2007). doi:10.1016/j.postharvbio.2007.06.024
17. D. Lorente, N. Aleixos, J. Gómez-Sanchis et al., Recent advances and applications of hyperspectral imaging for fruit and vegetable quality assessment. Food Bioprocess Technol. **5**, 1121 (2012). doi:10.1007/s11947-011-0725-1
18. A. Momose, W. Yashiro, H. Kuwabara et al., Grating-based X-ray phase imaging using multiline X-ray source. J. Appl. Phys. **48**, 076512 (2009). doi:10.1143/JJAP.48.076512
19. W. Yashiro, Y. Takeda, A. Momose, Efficiency of capturing a phase image using cone-beam X-ray Talbot interferometry. JOSA A **25**, 2025 (2008). doi:10.1364/JOSAA.25.002025
20. W. Sheng-Hao, M.P. Olbinado, A. Momose et al., Experimental research on the feature of an X-ray Talbot–Lau interferometer versus tube accelerating voltage. Chin. Phys. B **24**, 068703 (2015). doi:10.1088/1674-1056/24/6/068703
21. J. Brunner-Popela, O. Glatter, Small-angle scattering of interacting particles. I. Basic principles of a global evaluation technique. J. Appl. Crystallogr. **30**, 431 (1997). doi:10.1107/S0021889896015749
22. X. Song, B.W. Pogue, S. Jiang et al., Automated region detection based on the contrast-to-noise ratio in near-infrared tomography. Appl. Opt. **43**, 1053 (2004). doi:10.1364/AO.43.001053